HHS Public Access

Author manuscript

Science. Author manuscript; available in PMC 2017 June 24.

Published in final edited form as:

Science. 2016 June 24; 352(6293): 1535–1542. doi:10.1126/science.aaf7419.

A sentinel goblet cell guards the colonic crypt by triggering Nlrp6-dependent Muc2 secretion

George M.H. Birchenough, **Elisabeth E.L. Nyström**, **Malin E.V. Johansson**, and **Gunnar C. Hansson***

Department of Medical Biochemistry, University of Gothenburg, 40530 Gothenburg, Sweden

Abstract

Innate immune signaling pathways contribute to the protection of host tissue when bacterially challenged. Colonic goblet cells are responsible for generating the two mucus layers that physically separate the luminal microbiota from the host epithelium. We report the identification of a 'sentinel' goblet cell (senGC) localized to the colonic crypt entrance. This cell non-specifically endocytoses and reacts to TLR2/1, TLR4 and TLR5 ligands by activating the NLRP6 inflammasome downstream of TLR-MyD88-dependent Nox/Duox ROS synthesis. This triggers Ca^{2+}-dependent compound MUC2 exocytosis from the senGC and generates an intercellular gap junction signal that induces MUC2 secretion from adjacent goblet cells in the upper crypt which expels bacteria. Thus, senGCs guard and protect the colonic crypt from bacterial intruders that have penetrated the inner mucus layer.

The intestinal epithelium separates the luminal microbiota from the systemic tissues but is not the first line of defense. This function falls to the colonic mucus layers that are composed of polymeric sheets of MUC2 mucin (*1, 2*). The colonic mucus has an inner layer formed of closely packed MUC2 sheets and a less organized outer layer. The inner layer is impenetrable to bacteria, whereas the outer serves as a habitat for the microbiota (*1*). Deletion of Muc2 in mice eliminates the mucus causing bacterial colonization of the crypts, inflammation and carcinogenesis (*1, 3*). The mucus layers are vital for preventing colitis, but must function cooperatively with other elements of the epithelial innate immune system. These include TLR-MyD88 signaling and the NLRP6 inflammasome, as deletion of either renders the host susceptible to severe experimental colitis (*4-7*).

Mucus components, including MUC2, are produced by intestinal goblet cells (GCs). As GCs migrate up the colonic crypt they manufacture, store, and release MUC2 by regulated secretion. The colonic surface GCs continuously secrete MUC2 and maintain the mucus layers (*8*). Colonic GCs express Tlrs, MyD88 and the Nlrp6 inflammasome (*9, 10*). Thus, the crucial platforms for tissue preservation under challenge are expressed by the GCs.

***Correspondence: gunnar.hansson@medkem.gu.se**.

Supplemental MATERIAL
www.sciencemag.org/XX
Materials and Methods
Reference 28
Figs. S1 – S7
Movies S1 - S7

Endogenous factors (e.g. acetylcholine) trigger MUC2 secretion from colonic GCs (*11, 12*); however, it is unknown if microbial TLR-ligands, for example lipopolysaccharide (LPS) or lipoteichoic acid (LTA), might regulate mucin secretion. .

Bacterial TLR-ligands induce Muc2 secretion

The capacity of bacterial TLR-ligands to stimulate Muc2 secretion from colonic GCs was initially investigated (Fig. 1A). Using dynamic changes in explant mucus thickness as an indicator of secretion (*12, 13*) we observed that LTA, bacterial DNA and the peptidoglycan subcomponents muramyl dipetide (MDP) and g-D-glutamyl-meso-diaminopimelic acid (iE-DAP) failed to elicit any secretory response. Conversely LPS, its subcomponent Lipid A, the triacylated lipopeptide P3CSK4, and flagellin all stimulated an increase in mucus thickness similar to the acetyl choline analogue carbachol (CCh). LPS and P3CSK4 treatment of intact colonic tissue verified that the effect was not related to *ex vivo* muscle removal (Fig. S1A). Ileal GCs are also responsive to CCh treatment (*12*), but were insensitive to LPS, P3CSK4 and flagellin (Fig. 1B).

Mucus quantified in the tissue explant system is dependent on Muc2 (i.e. completely absent in *Muc2*$^{-/-}$ tissue) and alterations in mucus thickness are primarily reflective of Muc2 secretion. However, mucus thickness alterations may also be affected by volume expansion. Trans-epithelial potential difference (PD) recordings indicated transient ionic flux after treatment with LPS (Fig. 1C). A similar effect has been linked to cholinergic Muc2 secretion (*12*). Imaging of colonic explants from an mCherry-MUC2 expressing transgenic mouse (RedMUC2^{98trTg}) revealed secreted MUC2 only in treated tissues (Fig. 1D). As mucus expands in volume it becomes more penetrable to bacterial-sized beads. The thickness of mucus increased after LPS treatment, but no evidence of increased penetrability was observed (Fig. 1E, F). Thus, bacterial Tlr-ligands induced Muc2 secretion.

Colonic GCs are likely routinely exposed to high concentrations of the TLR-ligands that stimulated Muc2 secretion *ex vivo*. To examine the *in vivo* activity of TLR-ligand induced secretion the sensitivity of the response was examined (Fig. 1G). Similar response curves were produced for Lipid A, P3CSK4 and flagellin with EC50 values between 0.4-0.85 μM. To assess this sensitivity in the appropriate biological context, the concentration of soluble Lipid A in two colonic luminal compartments, the stool and mucus, was estimated by Limulus Amebocyte Lysate (LAL) assay (Fig. 1H). LAL reactivity of stool was 360-fold higher than that of mucus, indicating a steep gradient in Lipid A concentration between the mucus and the stool. This reflected the 210-fold difference in bacterial 16S load between these compartments (Fig. 1I). LAL reactivity to 0.85 μM (EC50) Lipid A was 20-fold less than LAL reactivity to stool and 18-fold higher than LAL reactivity to mucus (Fig. 1H). Estimated *in vivo* Lipid A concentrations were plotted on the Lipid A response curve and closely mirrored the response window (Fig. 1G). These results showed that the TLR-ligand triggered Muc2 secretion in the distal colon was inactive under normal conditions as the mucus layer close to the colonic GCs did not harbor sufficient Lipid A concentrations to trigger secretion.

TLR-ligands induce Muc2 secretion in specific GCs

Intestinal GCs are more functionally heterogeneous than previously expected (*8, 9*). We therefore tested whether TLR-ligands induced Muc2 secretion from a specific population of GCs. RedMUC2^{98trTg} colonic explants were treated with LPS, P3CSK4, flagellin or CCh individually or in combination, and tissue sections were imaged (Fig. 2A, B). Untreated tissue had filled GCs in the upper crypt and less filled GCs in the lower crypt. Upper crypt GCs were emptied in tissues treated with TLR-ligands. Conversely, CCh treatment resulted in secretion of MUC2 at the lower crypt without affecting the upper crypt GCs. Combined treatment with LPS and CCh emptied both upper and lower crypt GCs. Mucus secretion was quantified from explants co-treated with LPS and either P3CSK4, flagellin or CCh (Fig. 2C). Combined LPS and P3CSK4/flagellin treatments did not induce any additive secretory response, whereas combined LPS and CCh treatment did. Reversing the direction (apical vs. serosal) of LPS and CCh treatment did not induce Muc2 secretion indicating that responses were compartmentalized (Fig. 2D). Together, these observations indicated that LPS, P3CSK4 and flagellin all induced MUC2 secretion from the same upper crypt GCs and that these cells were distinct from the GCs targeted by CCh.

Another apically exposed GC population are the inter-crypt GCs (*8*). These cells do not store large amounts of mature glycosylated Muc2 and are frequently not observed by conventional mucin staining. However, they can be identified in RedMUC2^{98trTg} tissues and are distinguishable from upper crypt GCs (Fig. 2E). Comparison of untreated and LPS treated tissue identified upper crypt GCs secreting MUC2 in LPS treated tissue, but did not show any alterations to the inter-crypt GCs. These results confirmed that only the upper crypt colonic GCs were responsive to LPS.

The Muc2 secretory signaling pathway

Colonic GCs express Tlrs that recognize LPS, P3CSK4 and flagellin (*9*), and the Nlrp6 inflammasome which has been suggested to regulate GC Muc2 secretion (*10*). To examine the role of these mediators in controlling TLR-ligand stimulated secretion, mucus secretion was quantified in colonic explants from a range of knockout (KO) mice (Fig. 3A).

LPS, P3CSK4 and flagellin are recognized by TLR4, TLR2/1 and TLR5 which activate signaling via proximal mediators such as MyD88 and TRIF. Loss of their cognate receptors and MyD88, but not TRIF, prevented both LPS and P3CSK4 induced secretion (Fig. 3A). *Tlr5*$^{-/-}$ tissue was not examined; however, the response to flagellin was not lost in *MyD88*$^{-/-}$ or *Trif*$^{-/-}$ tissues which indicated that TLR-MyD88/TRIF signaling was not essential to flagellin induced secretion. The response to all three TLR-ligands was preserved in *Rag1*$^{-/-}$ tissue, ruling out a role for mucosal lymphocytes in mediating Muc2 secretion (Fig. S1B). CCh responses were unaltered in any of the Tlr/MyD88/Trif/Rag1 KO tissues.

Examination of LPS, P3CSK4 and flagellin-induced mucus secretion in Nlrp deficient tissues precluded the involvement of Nlrp3 and Nlrc4, but indicated that Nlrp6-signaling was essential for the response to all three TLR-ligands (Fig. 3A). Similarly, no response was observed in *Caspase1/11*$^{-/-}$ and *Caspase11*$^{-/-}$ tissue. Caspase1-mediated maturation of IL1β

and IL18 is the conventional purpose of activated inflammasomes; the response to all three TLR-ligands was unaltered in *IL1α/β*$^{-/-}$ and *IL18*$^{-/-}$ tissue, indicating that Nlrp6 inflammasome signaling did not rely on IL1β and IL18.

It has been suggested that *Nlrp6*$^{-/-}$ and *Caspase1/11*$^{-/-}$ colonic GCs lack normal Muc2 secretion and an intact inner mucus layer (*10*), which could account for an inability to secrete Muc2. However, all of the different inflammasome KO tissues responded normally to CCh stimulation and all strains had an intact inner mucus layer when housed in our facility (Fig. S2).

To dissect the cellular responses involved in TLR-ligand-induced Muc2 secretion we tested inhibitors targeting various cellular processes (Fig. 3B). Dynasore, which inhibits endocytosis, blocked the response to both LPS and P3CSK4, but not flagellin. Identical results were obtained by inhibition of NADPH/Dual oxidase (Nox/Duox) reactive oxygen species (ROS) synthesis using diphenyleneiodonium (DPI). Peptide-mediated inhibition of Caspase1/11 activation mimicked results from Caspase KO tissue, confirming the necessity for inflammasome activation. Atropine, a pan-muscarinic acetyl choline receptor inhibitor, blocked CCh induced secretion, but had no effect on tissue responses to TLR-ligands.

ROS synthesis by Nox/Duox can be activated downstream of TLR-signaling and act as an upstream stimulator of inflammasome activation (*14, 15*). DPI is a potent Nox/Duox inhibitor, but can also inhibit mitochondrial ROS release. We clarified this element of the pathway using N-acetyl cysteine (NAC), a non-specific ROS scavenger, and Mito-TEMPO, a ROS scavenger that accumulates in mitochondria (Fig. 3C). NAC prevented LPS stimulated Muc2 secretion whereas Mito-TEMPO had no effect, thus Nox/Duox was the likely source of LPS induced ROS synthesis. The fluorogenic ROS probe DCFDA was used to quantify LPS-induced ROS production in isolated colonic epithelial cells (Fig. 3D). ROS production was observed when cells were treated with LPS, and was inhibited by Dynasore, a MyD88 inhibitory peptide, DPI and NAC, but not the Caspase inhibitory peptide. This showed that LPS-induced ROS synthesis was dependent on endocytosis and MyD88-signaling, but was upstream of inflammasome activation. Intriguingly, flagellin treatment also induced ROS synthesis, which was dependent on both endocytosis and MyD88-signaling (Fig. 3D), showing that flagellin could activate a similar pathway to LPS.

Co-treatment of RedMUC2^{98trTg} epithelial cells with Caspase1/11 inhibitory peptide and fluorescent LPS allowed imaging of endocytotic GCs without triggering Muc2 secretion (Fig. 3E). Intracellular LPS was observed in only a small population of GCs. Thus, the endocytosis-dependent ROS synthesis observed in DCFDA loaded cells was likely generated by these GCs and supported the idea that a distinct population of GCs was responsive to the TLR-ligands.

Together these results suggested that LPS, P3CSK4 and flagellin stimulated Muc2 secretion from responsive GCs via activation of the Nlrp6 inflammasome. LPS and P3CSK4-induced inflammasome activation occurred downstream of endocytosis and TLR-MyD88-induced ROS synthesis. Whilst it was apparent that endocytosis of flagellin could also induce TLR-MyD88-dependent ROS synthesis, it was also evident that flagellin-induced Muc2 secretion

was not contingent on this element of the pathway and we therefore focused our subsequent studies on the response to LPS and P3CSK4.

TLR-ligands are endocytosed by senGCs

To identify LPS and P3CSK4-sensitive GCs in intact colonic tissue, RedMUC2^{98trTg} colonic explants were treated with fluorescent LPS or P3CSK4 and tissue was imaged (Fig. 4A-D). GCs that had taken up LPS/P3CSK4 were found exclusively in the apical regions of the crypt. Intriguingly, there appeared to be very few of these cells, with less than one cell/crypt (Fig. 4E). These cells were not observed in tissues pre-treated with Dynasore, confirming the requirement for endocytosis. Inhibition of inflammasome activation significantly increased the number of endocytotic cells detected, as did loss of TLR- or MyD88-signaling (Fig. 4B, E). This suggested that LPS/P3CSK4-triggered TLR-signaling and inflammasome activation resulted in loss of detectable endocytotic cells. This was investigated by treating explants with non-immunogenic dextran. Dextran was also taken up by a small number of GCs, but without inducing the same loss of endocytotic cells as LPS/P3CSK4 treatment (Fig. 4C, E). GCs which endocytosed dextran were identified as the same cells that endocytosed P3CSK4 (Fig. 4D) and examination of sections obtained from dextran treated tissue demonstrated that endocytosis was entirely restricted to GCs in the upper crypt region (Fig. S3A). To ensure that GC endocytosis observed *ex vivo* reflected processes occurring *in vivo*, dextran was administered intrarectally to live RedMUC2^{98trTg} mice. Uptake of dextran was again observed in a limited number of upper crypt GCs, confirming *ex vivo* observations (Fig. S3B).

Thus, luminal material was non-specifically endocytosed by a small subpopulation of upper crypt GCs. These cells were lost after TLR-MyD88 signaling and activation of the inflammasome. Crucially, only one or two such cells were typically detected per crypt. As this is only a fraction of the GCs which secreted in response to TLR-ligands this suggested that activation of endocytotic GCs must control secretion from other responsive, but not endocytotic, upper crypt GCs. The sampling and recognition of non-endogenous material is vital to the surveillance function of many types of host sentinel cell. As this process was apparent in the endocytotic GC this cell was named sentinel GC (senGC) to distinguish it from other upper crypt GCs.

Activated senGCs control Muc2 secretion

We examined the fate of senGCs lost after treatment and identified shed cells containing LPS or P3CSK4 and residual MUC2 suggesting that these were expelled senGCs (Fig. 5A). These were not present in tissue treated with dextran, indicating that expulsion was dependent on TLR engagement. Expelled cells were associated with diffuse extracellular MUC2 that was continuous with the remaining intracellular material (Fig. 5B). This implied that senGCs had undergone compound exocytosis (*16*) as well as being expelled. Intrarectal administration of P3CSK4 to live WT and RedMUC2^{98trTg} mice demonstrated that epithelial expulsion of GCs that had endocytosed P3CSK4 could also be observed *in vivo* (Fig. S4A, B). Intrarectal treatment of *Nlrp6*$^{-/-}$ mice identified cells that had endocytosed

P3CSK4, but did not induce epithelial expulsion (Fig. S4C). This confirmed that epithelial expulsion of senGCs was driven by Nlrp6 inflammasome activation.

Inflammasome activity was assessed using a fluorogenic peptide probe targeting active Caspase1 and Caspase11 (Casp1/11 FP). Tissue was loaded with Casp1/11 FP and then treated with LPS (Fig. 5C). Inflammasome activity was exclusively localized to cells that had been expelled from the upper crypt. Imaging of RedMUC2^{98trTg} tissue demonstrated that these cells were senGCs. Expelled senGCs were associated with long plumes of secreted MUC2 which confirmed that LPS treatment had triggered compound MUC2 exocytosis. No inflammasome activity or cellular expulsion was observed after LPS treatment of *Caspase1/11*$^{-/-}$ or *Nlrp6*$^{-/-}$ tissue, but both were detected in treated *Nlrp3*$^{-/-}$ tissue. This demonstrated that activity observed in these cells was specifically dependent on a functional Nlrp6 inflammasome.

senGC-mediated secretion was studied by live-imaging of RedMUC2^{98trTg} colonic explants. This revealed loss of MUC2 from upper crypt GCs in LPS or P3CSK4, but not in vehicle treated tissues (Movies S1, S2). Rapid MUC2 degranulation and epithelial expulsion was observed in a limited number of GCs per crypt (Fig. 5D; Movies S3, S4). Expulsion was used to designate the senGC and the remaining upper crypt GCs could be classified as ‘responsive’ or ‘non-responsive’ based on whether or not they secreted MUC2 (Fig. 5D). MUC2 fluorescence was subsequently quantified from different classes of GC and tracked over time (Fig. 5E, F; Movies S5, S6). Strikingly, this revealed that LPS/P3CSK4-induced MUC2 secretion was sequential in nature. Degranulation occurred initially in senGCs and then in responsive GCs. Responsive GC secretion occurred in sequence, starting with cells closest to the senGC and progressing around the crypt (Fig. 5F). This indicated that activated senGCs triggered an intercellular signal that induced MUC2 secretion in adjacent responsive GCs.

Intercellular senGC signaling

Localized intercellular signals can utilize paracrine or juxtacrine mechanisms. The mammalian intestine is highly innervated and paracrine signals can be generated by the enteric nervous system (ENS). Juxtacrine signals can be transmitted directly via intercellular cytoplasmic bridges formed by gap junction (GJ) connexons. We measured mucus secretion in colonic explants treated with inhibitors targeting each process. Tetrodotoxin (TTx) blocks ENS signaling, and carbenoxolone (CBX) can reduce GJ conductivity. Neither inhibitor affected CCh induced secretion; however, whilst TLR-ligand-induced secretion was unaffected by TTx, the response was blocked by CBX (Fig.5G). To verify GJ decoupling a fluorescence recovery after photobleaching (FRAP) assay was used to measure GJ conductivity. Vehicle or CBX treated explants were loaded with a GJ permeable dye and areas of epithelium were photobleached (Fig. S5A, B). Fluorescent recovery was significantly reduced in CBX compared to vehicle treated explants, indicating that GJ conductivity had been inhibited and supporting a role for GJ-signaling in controlling responsive GCs.

A recognized form of GJ-signaling is mediated by calcium. Increased cytosolic Ca^{2+} is derived from extracellular influx or release from ER stores via IP_3R or RyR channels. To investigate the role of Ca^{2+}-signaling in TLR-ligand-induced secretion, explants were pretreated with inhibitors prior to treatment with LPS or CCh (Fig. 5H). Cell permeable Ca^{2+}-chelator BAPTA-AM blocked secretion induced by either molecule, demonstrating the requirement for Ca^{2+}-release in both types of secretion. Cell impermeable Ca^{2+}-chelator EGTA only inhibited the response to LPS. Intracellular Ca^{2+}-store release was targeted by the RyR inhibitor Ryanodine and IP_3R inhibitor Xestospongin C (XeC). Inverse results were obtained for LPS and CCh with the LPS-dependent on IP_3R and CCh on RyR mediated Ca^{2+}-release. The requirement for Ca^{2+} influx and intracellular store release indicated that Ca^{2+}-induced Ca^{2+} release was active in LPS-induced secretion. To probe the sequence of Ca^{2+}-signaling events the Ca^{2+} ionophore Ionomycin was utilized (Fig. S5C). Ionomycin transports Ca^{2+} across membranes mimicking the Ca^{2+} influx required for LPS-induced secretion. Ionomycin induced MUC2 secretion and was insensitive to inhibition of ROS synthesis and inflammasome activation, but was inhibited by EGTA and XeC. This suggested that Ca^{2+} influx has a role upstream of Ca^{2+} store release and that direct induction of Ca^{2+}-signaling negates the requirement for inflammasome activation.

Ca^{2+}-signaling was imaged in LPS treated RedMUC2^{98trTg} colonic explants using the fluorogenic Ca^{2+}-indicator Fluo4 (Fig. 5I, J). Fluo4 positive GCs were observed after LPS but not vehicle treatment, indicating that LPS-induced Ca^{2+}-signaling could be visualized *ex vivo*. senGCs appeared to have higher Fluo4 signal compared to the responsive GCs where the signal was relatively weak (Fig. 5J; Movie S7). Sequential increases in cytoplasmic Ca^{2+} starting at the senGC appeared to follow the same pattern as observed for MUC2 secretion.

SenGCs flushes bacteria away from crypt openings

Induced Muc2 secretion may remove bacteria from the crypt opening and we tested this in our *ex vivo* tissue system. The inner mucus layer normally separates bacteria from the colonic tissue surface; therefore, this was first mechanically removed. Fluorescent bacteria were then applied to the tissue surface. Muc2 secretion was triggered by treatment with LPS and images of tissue and bacteria were acquired and bacterial spatial distribution quantified (Fig. 6A, B). Initially bacteria were identified at the tissue surface and close to the crypt openings. Treatment with LPS, but not vehicle, caused bacteria to be displaced from the crypt openings. Most bacteria remaining at the tissue surface after LPS treatment were in the inter-crypt regions, thus supporting the notion that this mechanism functions to specifically protect the crypts *in vivo*.

Oral DSS allow colonic bacteria to penetrate the inner mucus layer and contact the epithelium prior to the onset of inflammation (*17*). If senGCs protect the crypt from bacteria we hypothesized that DSS treatment should trigger senGC activation *in vivo*. Short-term (84 h) DSS treatment did not cause weight alterations (Fig. S6A). However, the inner mucus layer became partially penetrable to bacteria sized beads after 12 h of DSS treatment and was largely disrupted after 84 h (Fig. 6C). Casp1/11 FP probe was used to quantify epithelial inflammasome activation (Fig. 6D, S6B). This was detected in multiple cells after 12 h DSS treatment, but the number of these cells then declined. Inflammasome activity was

visualized in both upper crypt and shed cells with GC-like morphology (Fig. 6E) indicating that DSS had resulted in activation and epithelial expulsion of senGCs. That DSS treatment caused depletion of senGCs was confirmed by the loss of dextran endocytosis by upper crypt cells after 36 h (Fig. 6F). Endocytotic cells were clearly identified in untreated tissue but largely absent in tissue exposed to DSS indicating that the senGCs had been activated and depleted.

Normally colonocytes are separated from the microbiota by the inner mucus layer and disruption of this allows bacteria to approach the crypts (*1, 18-20*) (Fig. S7AB). Influx of bacteria increases the concentration of TLR-ligands near the crypt and activates senGCs (Fig. S7C). This is initiated by TLR-MyD88 signaling downstream of endocytosis, preceding Nox/Duox ROS synthesis and Nlrp6 inflammasome activation. This causes Ca^{2+}-signaling driving compound Muc2 secretion, generation of GJ-dependent intercellular signaling, Muc2 secretion from responsive GCs, and the expulsion of the activated senGC. This clears bacteria from the crypt opening (Fig. S7D), thereby protecting the lower crypt and intestinal stem cells from bacterial intrusion. Mouse strains unable to trigger senGC activation had a functional inner mucus layer, suggesting that senGCs are less important for normal mucus layer generation.

The pathway activating senGCs is supported by other observations as colonic GCs express the expected TLR repertoire and can take up luminal material (*9, 21, 22*). MyD88-signaling can induce Nox/Duox ROS synthesis (*23*) that has been coupled to inflammasome activation (*14, 15*) and was recently linked to GC endocytosis and autophagy (*24*). The senGC Nlrp6 inflammasome activation resulted in expulsion of these cells, a mechanism that could be important for clearing infected cells (*25, 26*) and blocking the crypt.

Administration of DSS to mice is a commonly used colitis model. DSS disrupts the inner mucus layer allowing bacteria to access the epithelial surface before onset of inflammation (*17*). Increased sensitivity to DSS treatment in animals lacking senGC activation mediators may be related to loss of senGC activity (*4, 5, 27*). DSS triggers inflammasome activity localized to upper crypt cells and leads to depletion of senGCs (Fig. 6C-F). *Ex vivo* experiments confirmed that senGC mediated mucus secretion displaced bacteria from crypt openings (Fig. 6A, B) and senGC activation after inner mucus layer disruption likely generates similar response. Depletion of senGCs by repeated challenge would leave the crypt without defense, an event that may be important in understanding the development of chronic colitis.

Supplementary Material

Refer to Web version on PubMed Central for supplementary material.

Acknowledgements

Supported by Swedish Research Council, Swedish Cancer Foundation, Knut and Alice Wallenberg Foundation, Lundberg Foundation, Sahlgren's University Hospital (ALF), Torsten Söderbergs Stiftelse, NIH-NIAID (U01AI095473), and Swedish Foundation Strategic Research. We acknowledge Gothenburg CCI for technical help, Frida Svensson for generating the RedMUC2^{98trTg} mice, and Wolf-Dietrich Hardt and MIVAC for mouse strains.

References AND NOTES

1. Johansson MEV, et al. Proc. Natl. Acad. Sci. USA. 2008; 105:15064–15069. [PubMed: 18806221]
2. Ambort D, et al. Proc. Natl. Acad. Sci. U. S. A. 2012; 109:5645–5650. [PubMed: 22451922]
3. Velcich A, et al. Science. 2002; 295:1726–1729. [PubMed: 11872843]
4. Rakoff-Nahoum S, et al. Cell. 2004; 118:229–241. [PubMed: 15260992]
5. Frantz AL, et al. Mucosal Immunol. 2012; 5:501–512. [PubMed: 22491177]
6. Lamkanfi M, Dixit VM. Cell. 2014; 157:1013–1022. [PubMed: 24855941]
7. Elinav E, et al. Cell. 2011; 145:745–757. [PubMed: 21565393]
8. Johansson MEV. PLoS ONE. 2012; 7:e41009. [PubMed: 22815896]
9. Knoop KA, et al. Mucosal Immunol. 2015; 8:198–210. [PubMed: 25005358]
10. Wlodarska M, et al. Cell. 2014; 156:1045–1059. [PubMed: 24581500]
11. Halm DR, Halm ST. Am J Physiol. 1999; 277:C501–C522. [PubMed: 10484337]
12. Gustafsson JK, et al. Am. J. Physiol. 2012; 302:G430–G438.
13. In Supplementary Materials
14. Zhou R, et al. Nat Immunol. 2010; 11:136–140. [PubMed: 20023662]
15. Bauernfeind F, et al. J Immunol. 2011; 187:613–617. [PubMed: 21677136]
16. Specian D, Neutra MR. J. Cell Biol. 1980; 85:626–640. [PubMed: 7391135]
17. Johansson MEV, et al. PLoS ONE. 2010; 5:e12238. [PubMed: 20805871]
18. Jakobsson HE, et al. EMBO Reports. 2015; 16:164–177. [PubMed: 25525071]
19. Johansson MEV, et al. Gut. 2014; 213:281–291.
20. Bergstrom KSB, et al. PLoS Pathog. 2010; 6:e1000902. [PubMed: 20485566]
21. McDole JR, et al. Nature. 2012; 483:345–349. [PubMed: 22422267]
22. Colony PC, Specian RD. Anat. Rec. 1987; 218:365–372. [PubMed: 3662039]
23. Panday A, Sahoo MK, Osorio D, Batra S. Cell Mol Immunol. 2015; 12:5–23. [PubMed: 25263488]
24. Patel KK, et al. Embo J. 2013; 32:3130–3144. [PubMed: 24185898]
25. Sellin ME, et al. Cell Host & Microbe. 2014; 16:237–248. [PubMed: 25121751]
26. Knodler L, et al. Cell Host & Microbe. 2014; 16:249–256. [PubMed: 25121752]
27. Demon D, et al. Mucosal Immunol. 2014; 7:1480–1491. [PubMed: 24850431]
28. Zoetendal EG, et al. Nature Protocols. 2006; 1:870–873. [PubMed: 17406319]

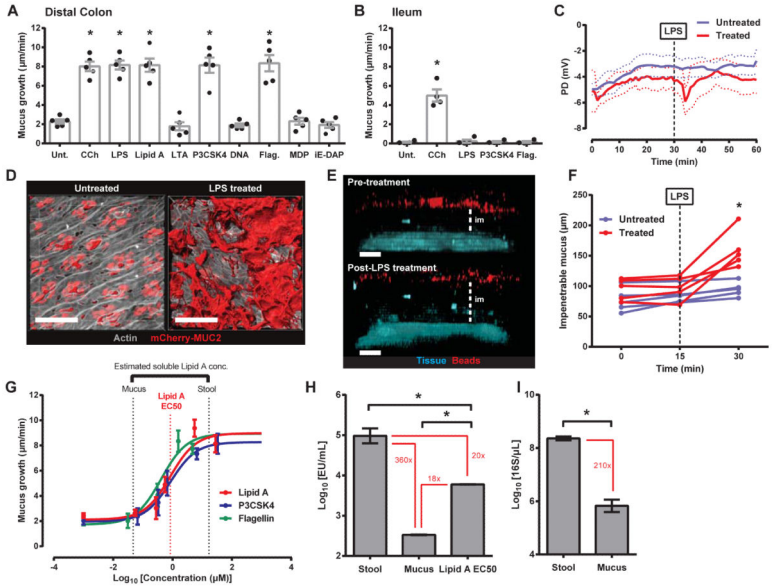

Fig. 1. Select TLR-ligands induce Muc2 secretion in distal colon

(**A-G**) Intestinal explants treated with TLR-ligands or carbachol. (**A, B**) Quantification of mucus growth from distal colonic (A) or ileal (B) explants: untreated (Unt.), flagellin (Flag.). (**C**) PD measurement. (**D**) Confocal micrographs of RedMUC2^{98trTg}: actin (grey), mCherry-MUC2 (red). (**E**) Confocal z-stacks of tissue and 1 µm beads: tissue (blue), beads (red), impenetrable mucus (im). (**F**) Impenetrable mucus thickness. (**G**) Concentration-response curves: Lipid A EC50 (red dashed line), estimated mucus and stool Lipid A concentrations (black dashed lines). (**H**) LAL reactivity of stool, mucus, and Lipid A EC50 (0.85 µM): indicated fold differences between data (red). (**I**) Quantification of 16S in stool and mucus by qPCR: indicated fold differences (red). Errors SEM of 4-5 animals; significance by Dunnett (A, B, H), Sidak (F) or Mann-Whitney (I) test (* p<0.05); scales 50 µm.

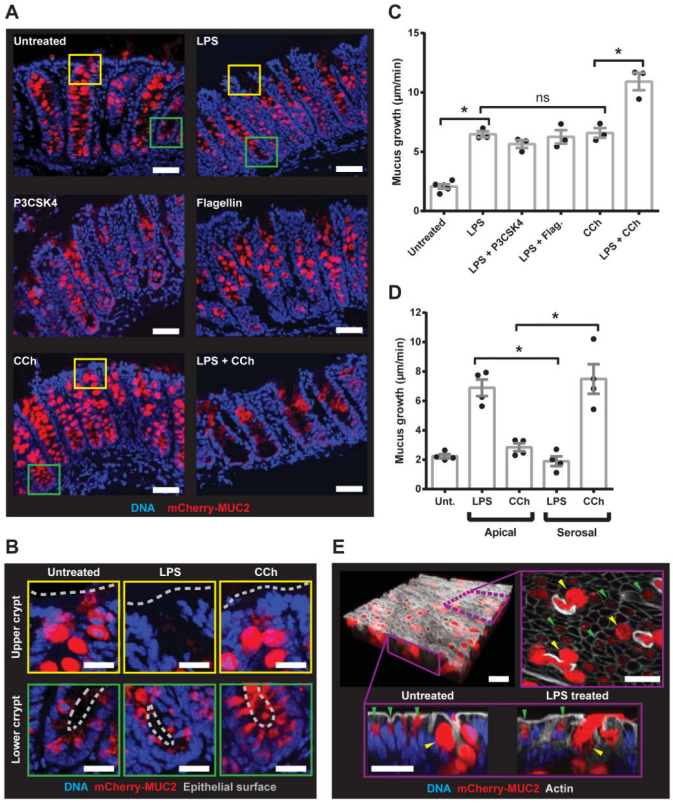

Fig. 2. TLR-ligand responsive GCs are localized to the upper crypt

(**A-E**) Colonic explants were treated with TLR-ligands or CCh (**A**) Confocal micrographs of cryosections from RedMUC2^{98trTg}: MUC2 (red), DNA (blue). (**B**) Magnified upper crypt (yellow boxes) or lower crypt (green boxes) in (A): epithelial surface (grey line). (**C, D**) Quantification of mucus growth rates. (**E**) Upper crypt GCs (yellow arrows) and inter-crypt GCs (green arrows) in RedMUC2^{98trTg} colon: confocal z-stack of tissue surface (upper left), x/y-axis cross-section (upper right), x/z-axis cross-sections (lower left/right), DNA (blue), mCherry-MUC2 (red), actin (grey). Errors SEM of 3-4 animals; significance by Tukey's multiple comparison (* p<0.05). Scales 50 µm (A) or 20 µm (B, E).

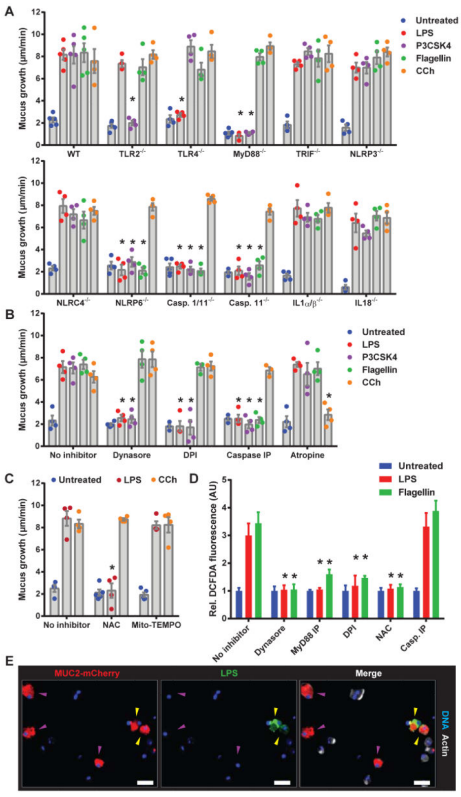

Fig. 3. TLR-ligand driven Muc2 secretion requires endocytosis, signaling and ROS synthesis upstream of inflammasome activation

Colonic explants (**A-C**) or cell suspensions (**D, E**) were treated with TLR-ligands or CCh. (**A**) Quantification of mucus growth in WT or KO or (**B**) pre-treated with inhibitors. (**C**) Quantification of mucus growth pre-treated with ROS scavengers. (**D**) DCFDA-fluorescence in epithelial cells pre-treated with inhibitors. (**E**) Confocal micrographs of RedMUC2^{98trTg} epithelial cells with Caspase inhibitory peptide (Casp. IP): non-endocytotic GCs (purple arrows), endocytotic GCs (yellow arrows), mCherry-MUC2 (red), DNA (blue) actin (grey). Errors SEM of 4-5 animals; significance by Dunnett's multiple comparison of WT vs. KO (A) or no inhibitor vs. inhibitor (B, C, D) data (* p<0.05). Scales 50 μm.

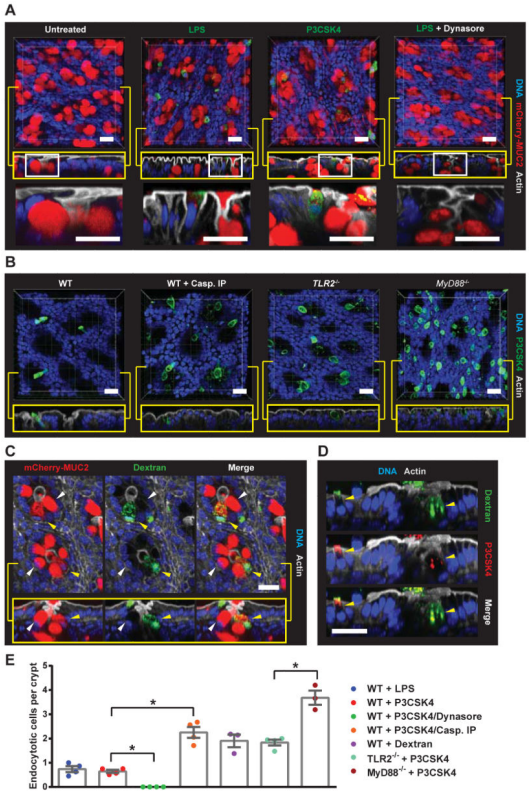

Fig. 4. TLR-ligands are endocytosed by a sentinel GC

(**A-D**) Colonic explants were treated as indicated, whole mounted and visualized by confocal microscopy: (A-C) x/y-axis cross-sections (upper), x/z-axis cross-sections (yellow boxes), DNA (blue), actin (grey). (**A**) RedMUC2^{98trTg} tissue: magnified x/z-axis cross-section regions indicated by white boxes (lower), LPS/P3CSK4 (green), mCherry-MUC2 (red). (**B**) WT with or without Casp. IP, *Tlr2*$^{-/-}$, and *MyD88*$^{-/-}$ tissue: P3CSK4 (green). (**C**) RedMUC2^{98trTg} tissue: endocytotic GC (yellow arrow), non-endocytotic GC (white arrow), mCherry-MUC2 (red), dextran (green). (**D**) P3CSK4/dextran co-treated WT colon. (**E**) Quantification of endocytotic cells. Errors SEM of 3-4 animals; significance by Tukey's multiple comparison (* p<0.05). Scales 20 μm.

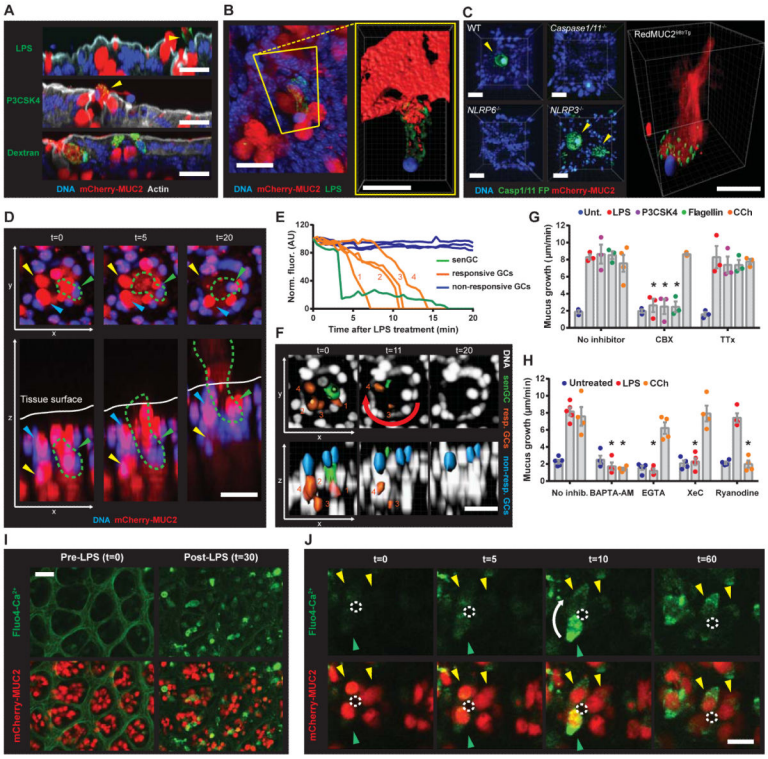

Fig. 5. Activated senGCs are expelled from the epithelium and trigger GJ and Ca^{2+}-dependent Muc2 secretion from responsive upper crypt GCs

(**A-J**) Colonic explants were treated with TLR-ligands or CCh. (**A, B**) RedMUC2^{98trTg} tissue whole mounts visualized by confocal microscopy: DNA (blue), actin (grey), mCherry-MUC2 (red), LPS/P3CSK4/dextran (green). (**A**) x/z-axis cross-sections showing expelled senGCs (yellow arrows). (**B**) Expelled senGC overview (left panel) and isosurface enhanced view (right panel, yellow box). (**C**) Localization of inflammasome activity after LPS treatment of WT, KO and RedMUC2^{98trTg} tissue: Caspase1/11 fluorogenic probe (Casp1/11 FP, green), DNA (blue), senGCs (yellow arrows). (**D-F**) RedMUC2^{98trTg} tissue imaged by confocal microscopy (**D**) x/y-axis (upper) and x/z-axis views (lower) of a crypt at different time-points after LPS treatment: senGC (green arrow, green dashed line), responsive GC (yellow arrow), non-responsive GC (blue arrow). (**E**) Quantification of mCherry-MUC2 fluorescence of individual GCs from crypt in (D). (**F**) Fluorescent isosurfaces used to generate data in (E), responsive GC numbering corresponds to plots in (E), sequence of responsive cell secretion (red arrow): DNA (white), senGC (green), responsive GCs (orange), non-responsive GCs (blue). (**G, H**) Quantification of mucus growth with or without carbenoxolone (CBX), tetrodotoxin (TTx) or Ca^{2+}-signaling inhibitors. (**I, J**) RedMUC2^{98trTg} tissue loaded with fluorogenic Ca^{2+} indicator (Fluo4) and imaged by confocal microscopy: Fluo4 (green), mCherry-MUC2 (red). (**I**) x/y-axis view of tissue pre- and post-treatment. (**J**) x/y-axis view of a crypt at different time-points after LPS treatment: sequence of GC secretion (white arrow), crypt opening (white dashed line), senGC (green arrow), responsive GCs (yellow arrows). Errors SEM of 4-5 animals; significance by Dunnett's multiple comparison (* p<0.05). Scales 20 µm.

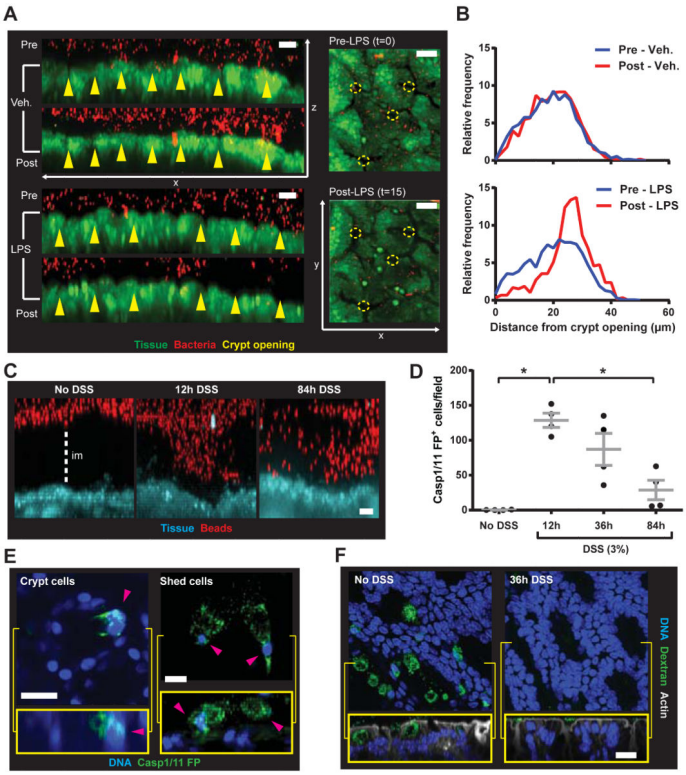

Figure 6. senGC activation removes bacteria from crypt openings *ex vivo* and is triggered by disruption of the inner colonic mucus layer *in vivo*

(**A**) Fluorescent bacteria (red) applied to colonic explant tissue (green) and imaged pre- (upper) and post- (lower) LPS or vehicle treatment: x/z-axis view (left), x/y-axis view (right), crypt openings (yellow arrows and circles). (**B**) Distribution of bacteria in relation to crypt openings as in (A). Data representative of 4 independent experiments. (**C-F**) Mice given 3% DSS in drinking water; samples collected after 0 (no DSS), 12, 36 and 84 h. (**C**) Confocal z-stacks of colonic explants and 1 μm beads: tissue (blue), beads (red), impenetrable mucus (im). (**D**) Quantification of cells with inflammasome activity (Casp1/11 FP^+) detected in live tissue. (**E**) Casp1/11 FP^+ cells (pink arrows) with GC morphology in the upper crypt (left) and shed from tissue (right): x/y-axis view (upper), x/z-axis view (lower). (**F**) Colonic explants were treated with fluorescent dextran, fixed, whole mounted, and visualized by confocal microscopy: x/y-axis view (upper), x/z-axis view (lower), DNA (blue), dextran (green), actin (grey). Errors SEM of 4 animals; significance by Dunn's multiple comparison (* $p<0.05$); scales 20 μm.